6-3-2019

Brainstem atrophy in focal epilepsy destabilizes brainstem-brain interactions: Preliminary findings.

Susanne G. Mueller
University of California, San Francisco

Lisa M. Bateman
Columbia University

Maromi Nei
Thomas Jefferson University, maromi.nei@jefferson.edu

Alica M. Goldman
Baylor Medical College

Kenneth D. Laxer
California Pacific Medical Center,

NeuroImage: Clinical 23 (2019) 101888

Contents lists available at ScienceDirect

NeuroImage: Clinical

journal homepage: www.elsevier.com/locate/ynicl

Brainstem atrophy in focal epilepsy destabilizes brainstem-brain interactions: Preliminary findings

Susanne G. Mueller[a,*], Lisa M. Bateman[b], Maromi Nei[c], Alica M. Goldman[d], Kenneth D. Laxer[e]

[a] Dept. of Radiology, University of California, San Francisco, CA, USA
[b] Dept. of Neurology, Columbia University, NY, USA
[c] Dept. of Neurology, Thomas Jefferson University, Philadelphia, PA, USA
[d] Dept. of Neurology, Baylor Medical College, Houston, TX, USA
[e] Pacific Epilepsy Program, California Pacific Medical Center, San Francisco, CA, USA

ARTICLE INFO

Keywords:
Brainstem
Network
Autonomic control
Gray matter
Connectivity
Functional

ABSTRACT

Background: MR Imaging has shown atrophy in brainstem regions that were linked to autonomic dysfunction in epilepsy patients. The brainstem projects to and modulates the activation state of several wide-spread cortical/subcortical regions. The goal was to investigate 1. Impact of brainstem atrophy on gray matter connectivity of cortical/subcortical structures and autonomic control. 2. Impact on the modulation of cortical/subcortical functional connectivity.

Methods: 11 controls and 18 patients with non-lesional focal epilepsy (FE) underwent heart rate variability (HRV) measurements and a 3 T MRI (T1 in all subjects, task-free fMRI in 7 controls/ 12 FE). The brainstem was extracted, and atrophy assessed using deformation-based-morphometry. The age-corrected z-scores of the mean Jacobian determinants were extracted from 71 5x5x5 mm grids placed in brainstem regions associated with autonomic function. Cortical and non-brainstem subcortical gray matter atrophy was assessed with voxel-based-morphometry and mean age corrected z-scores of the modulated gray matter volumes extracted from 380 cortical/subcortical rois. The profile similarity index was used to characterize the impact of brainstem atrophy on gray matter connectivity. The fMRI was preprocessed in SPM12/Conn17 and the BOLD signal extracted from 398 ROIs (16 brainstem). A dynamic task-free analysis approach was used to identify activation states. Connectivity HRV relationship were assessed with Spearman rank correlations.

Results: HRV was negatively correlated with reduced brainstem right hippocampus/parahippocampus gray matter connectivity in controls ($p < .05$, FDR) and reduced brainstem to right parietal cortex, lingual gyrus, left hippocampus/amygdala, parahippocampus, temporal pole, and bilateral anterior thalamus connectivity in FE ($p < .05$, FDR). Dynamic task-free fMRI analysis identified 22 states. The strength of the functional brainstem/cortical connectivity of state 15 was negatively associated with HRV ($r = -0.5$, $p = .03$) and positively with decreased brainstem-cortical (0.49, p = .03) gray matter connectivity.

Conclusion: The findings of this small pilot study suggest that impaired brainstem-cortex gray matter connectivity in FE negatively affects the brainstem's ability to control cortical activation.

1. Introduction

Sudden unexpected death in epilepsy (SUDEP) is defined as an unexpected, witnessed or unwitnessed death not related to a status epilepticus, drowning, suicide or an accident that occurs under benign circumstances in a person suffering from epilepsy. It is only surpassed by stroke in total potential years of life lost due to a neurological disease and is the leading cause of death in 10–50% of the patients with chronic drug-resistant epilepsy (Devinsky et al., 2016, Jones and Thomas, 2017, Thurman et al., 2014, Harden et al., 2017, Sveinsson et al., 2017). The small number of witnessed cases suggests that SUDEP occurs typically but not exclusively after a severe seizure (Ryvlin et al., 2013; Lhatoo et al., 2016). The first sign is an impaired responsiveness to the environment. Then it comes to a sudden breakdown of the autonomic system that is typically initiated by a disturbance of the respiratory function and followed by cardiac failure. Towards the end these symptoms are often accompanied by a generalized suppression of the EEG activity (Ryvlin et al., 2013).

* Corresponding author at: Center for Imaging of Neurodegenerative Diseases, VAMC San Francisco, 4150 Clement Street, San Francisco, CA 94121, USA.
E-mail address: susanne.mueller@ucsf.edu (S.G. Mueller).

https://doi.org/10.1016/j.nicl.2019.101888
Received 27 March 2019; Received in revised form 3 May 2019; Accepted 29 May 2019
Available online 03 June 2019

Table 1
Characteristics of ASF patient population.

Patient	Age at MRI	Age at Onset	Epilepsy Type	Epilepsy Syndome	Lateralization	Localization	MRI	Seizure Type
1	52	na	LRE	TLE	R	temporal	normal	CPS
2[c]	22	8	LRE	TLE	L	temporal	MTS	CPS
3[c]	54	15	LRE	TLE	R	temporal	normal	CPS
4	34	10	LRE	TLE	bil	temporal	normal	SPS,CPS
5[c]	64	na	LRE	TLE	L	temporal	MTS	SPS
6[c]	64	60	LRE	TLE	bil	fronto-temporal	normal	CPS
7[c]	25	childhood	LRE	TLE	R	temporal	MTS	CPS
8[a]	51	28	LRE	TLE	L	temporal	MTS	SPS, CPS
9[a]	25	19	LRE	TLE	L	temporal	normal	CPS SGTC
10	48	45	LRE	TLE	L	fronto-temporal	MTS	CPS
11[a]	29	< 1	LRE	TLE	R	fronto-temporal	MTS	SPS, CPS
12[a]	27	26	LRE	TLE	R	temporal	normal	SPS, CPS
13[c]	52	na	LRE	TLE	non lat	temporal	normal	SPS
14[c]	50	14	LRE	TLE	L	fronto-temporal	normal	CPS
15[c]	27	22	LRE	TLE	R	temporal	normal	SPS
16	31	childhood	LRE	TLE	non lat	temporal	normal	SPS, CPS
17	39	36	LRE	TLE	bil	temporal	normal	SPS, CPS
18[c]	29	28	LRE	TLE	L	temporal	normal	SPS, CPS

CPS, complex partial, SGTC, secondary generalized tonic clonic, SPS, simple partial, MTS, mesial temporal sclerosis.
R, right; bil, bilateral; L, left; non-lat, no lateralizing information in scalp EEG; na, non available,
[b] Therapy refractory epilepsy, evaluation for surgery.
[c] Rare seizures (< 3/year or SPS only).

The simultaneous disturbance of consciousness and autonomic control points to a pathological process in the brainstem. An involvement of the brainstem in the events leading to SUDEP is also supported by the findings in animal models of SUDEP (Holt et al., 2016), by MR studies describing more pronounced volume loss and network abnormalities extending in the lower brainstem in patients who later died of SUDEP (Mueller et al., 2014; Mueller et al., 2018) and by an autopsy study that found histopathological abnormalities in the lower brainstem of patients who had died of SUDEP that were absent in epilepsy patients who had died of other causes (Patodia et al., 2018). The regions highlighted by these studies encompass some of the brainstem's major serotoninergic, noradrenergic and cholinergic centers with widespread efferent and afferent connections not only between themselves but also with cortical/subcortical structures. Brainstem-brain interactions have been shown to modulate activity and neurotransmitter release of cortical and subcortical neurons and to generate activity states that critically influence attention, cognition, mood and impulse control by synchronizing and desynchronizing the firing of larger neuron populations (Puig and Gener, 2015; Celada et al., 2013; Venkatraman et al., 2017; deGee et al., 2017; Safaai et al., 2015; Neves et al., 2018). Given these widespread brainstem-brain interactions, one would expect structural and functional abnormalities at the brainstem level to be reverberated at the subcortical and cortical level and to play an important role in interictal and ictal disturbances of cognition, mood etc. Describing the combined impact of brainstem and cortical/subcortical structural and functional abnormalities will not only allow to better understand how they compromise autonomic function but could also provide new insights into the mechanisms of SUDEP. A small pilot study with 18 patients with focal epilepsy and 10 controls was undertaken to investigate this overarching goal. The first objective of this study was to characterize how volume loss in regions involved in autonomic control in the brainstem relates to volume loss in cortical/subcortical brain regions and to investigate how this pattern of volume loss affects autonomic control measured as heart rate variability (HRV) in patients with focal epilepsy. A new approach, the so-called atrophy profile similarity index (PSI) (Mueller and Weiner, 2017) combined with graph analysis was used to describe the pattern of volume loss. It was expected that this approach would highlight a network of subcortical and cortical regions rather than a single critical structure, e.g. the amygdala (Dlouhy et al., 2015). This network would encompass cortical/subcortical and brainstem structures that receive strong projections from each other, are known to be involved in autonomic control, and to be affected by the excitotoxic effects of seizures/seizures spread, i.e., hippocampus, amygdala, insula, cingulate and medial prefrontal regions. The second objective was to identify brain activity states associated with HRV and to investigate how structural brainstem-brain abnormalities influence the expression of these states. Task-free fMRI combined with a dynamic analysis approach consisting of a combination of graph analysis and hierarchical cluster analysis was used to identify different brain activity states based on their connectivity profiles. The hypothesis to be tested was that the duration and expression of brain activity states playing a role in the regulation of autonomic control are associated with HRV and that structural brainstem-brain network abnormalities modify these association, i.e., either suppress or facilitate the appearance of abnormal activity states.

2. Material and methods

2.1. Study population

The study population is identical with the Autonomic System Function population described in Mueller et al., 2018b. It consisted of 18 epilepsy patients (mean age: 40.2 (14.1) years, m/f: 9/9) suffering from non-lesional (exception mesial-temporal sclerosis) focal epilepsy (FE). The severity of their epilepsy ranged from therapy-refractory epilepsy to relatively well controlled epilepsy with occasional focal aware seizures. The localization of the epileptic focus was based on semiology and interictal and - if available - ictal EEG recordings, please see Table 1 for details. Eleven healthy controls (mean age: 30.7 (7.8), m/f: 6/5) had been recruited from the community for this project and underwent the same study procedures. To better capture the normal range of gray matter connectivity, they were complemented by a "reference population" consisting of 21 healthy subjects (mean age 26.2 (5.9)) who had been recruited for another project and had been studied on the same magnet with the same T1 sequence as the study population but had not undergone the other study specific procedures. The committee of human research at the University of California, San Francisco (UCSF) and the VA Medical Center had reviewed and approved the study. Informed consent in accordance with the Declaration from Helsinki had been obtained.

2.2. Heart rate variability (HRV)

All epilepsy and control subjects but not the reference population underwent an EEG recording (32 channels including one ECG channel) (BRAINAMP MR) before their MR exam. The EEG was set up in a dimly lighted room close to the MR suite and a short baseline EEG (5–10 min) in a relaxed, awake state with eyes closed was recorded before the patient was transferred to the MRI for the MR exam. All the exams took place in the mid-afternoon. The ECG obtained during this EEG was extracted and analyzed with Kubios HRV (version 2.1) software and heart rate (HR) and heart rate variability (HRV, defined as standard deviation of beat-to-beat intervals or SDNN) from artifact free sections calculated. The resulting raw HRV was converted into a heart-rate adjusted HRV z-score using the ranges of HR and HRV observed in the control group since initial analyses showed not only the expected dependency of HRV on HR but also a variation of the baseline HR in controls and patients (O'Brien and Dyck, 1995).

2.3. Imaging and image analysis

All images were acquired on a Siemens Skyra 3 T MR system equipped with a 20 channel receive coil. The following sequences were obtained as part of a larger research protocol in all subjects. 1. T1-weighted gradient echo MRI (MPRAGE) of entire brain, TR/TE/TI = 2300/2.96/1000 ms, $1.0 \times 1.0 \times 1.0\,mm^3$ resolution, acquisition time = 5.30 min for tissue segmentation. 2. PD/T2 weighted 2D turbo spin-echo sequence, TR = 3210, TE1/2 = 101/11 ms, $1.0 \times 1.0 \times 3.0\,mm^3$ resolution, acquisition time: 3.43 min. Nineteen subjects (7 controls and 12 FE) also underwent task-free fMRI using a 2D gradient echo EPI sequence with TR/TE = 2020/27 ms, flip angle = 77, $2.5 \times 2.5 \times 3$ mm resolution, no gaps, acquisition time = 8.00 min. Subjects were instructed to refrain from caffeinated beverages on the day of the exam, to close their eyes and to relax but stay awake and think of nothing in particular during the scan.

2.3.1. Structural imaging

2.3.1.1. Cortex, subcortical structures. Each subject's T1 image underwent tissue segmentation with the new segment algorithm as implemented in SPM12 (https://www.fil.ion.ucl.ac.uk/spm). The resulting gray matter maps were warped onto a symmetrical gray matter template using DARTEL as implemented in SPM12. The Jacobian determinants from the warping step were calculated and used to re-scale the gray matter maps. After smoothing with a 4 mm FWHM Gaussian kernel, ICV correction using the ICV volume calculated by FreeSurfer and normalization of the maps to the MNI space, age-corrected z-score maps were calculated using the ranges observed in the ICV corrected, spatially normalized and rescaled gray matter maps of the 11 control and 21 reference subjects (O'Brien and Dyck, 1995). The AICHA parcellation (Joliot et al., 2015) was used to extract the mean age corrected z-scores from 380 cortical and subcortical gray matter regions for each of the 18 FE and 11 controls with HRV measurements (please see Fig. 1, lower panel).

2.3.1.2. Brainstem. The T1 images were processed with FreeSurfer 5.3 (http://surfer.nmr.mgh.harvard.edu). The labels cerebellum gray and white, brainstem, left and right diencephalon and left and right thalamus produced by the FreeSurfer subcortical segmentation stream were used to generate a mask encompassing brainstem, cerebellum, diencephalon and thalamus for each subject. The accuracy of this mask was visually checked and manually edited if necessary to ensure that it covered all structures of interest equally well in all subjects before using it to extract the corresponding regions (brainstem plus) from each subject's bias corrected gray scale image. The resulting brainstem plus images from 11 healthy controls and 21reference subjects were used to generate a brainstem plus template using the shoot tools as implemented in SPM12 (run shooting, create template) (Ashburner and Friston, 2011). Each subject's brainstem plus image was warped onto this template using the high dimensional warping algorithm of the shoot toolbox and the Jacobian determinants were calculated. The resulting Jacobian maps were corrected for head size using the intracranial volume calculated by FreeSurfer and smoothed with a 4 mm FWHM Gaussian kernel. The resulting image was masked with a brainstem/diencephalon mask to remove the cerebellum and to suppress the background, and finally corrected for age by calculating age-corrected z-score maps using the ranges observed in the equally processed brainstem images of the 11 controls and 21 reference subjects (O'Brien and Dyck, 1995).

A 5x5x5 voxel grid system was overlaid on the brainstem plus template. Brainstem nuclei/regions involved in autonomic control are not distinguishable on a 3 T in vivo image nor on the T1 brainstem template. Therefore, macroscopic landmarks identified in the atlas of histological and 9.4 T high resolution sections of the brainstem/medulla (Naidich et al., 2009) were used to identify 71 regions of interest or structural rois (srois) that encompassed brainstem structures known to be involved in autonomic control or to play a role in animal models of SUDEP (e.g., N'Gouemo and Faingold, 2000; Kommajosyula et al., 2017; Zhang et al., 2018). These 71 srois included 19 srois in the nucleus ambiguus, nucleus of the solitary tract, dorsal motor nucleus of the vagus, hypoglossus, parabrachialis, caudal part of reticular formatio (autonomic), 10 srois in raphe nuclei or median reticular formation (raphe), 18 srois covering the central and lateral reticular formation (reticular), 6 srois in the region of the periaqueductal gray, 11 srois in the region of the superior/inferior colliculi and ventral tegmentum (colliculi & tegmentum) and 6 srois in tract regions, i.e., medial, lateral lemniscus, medial longitudinal fascicle (tract), please see Fig. 1. For the purpose of this study, 11 srois in the medulla oblongata and pontomedullary junction were assigned to a “lower brainstem” group and 16 srois in the mesencephalon were assigned to a “upper brainstem” group. The mean age-corrected z-scores of each of these 71 cROIs were calculated for the 18 FE and 11 controls with HRV measurements (please see Fig. 1, upper panel). The motivation to analyze all brainstem srois as well as restricting the analysis to upper and lower srois only was based on the findings in SUDEP patients reported in a previous publication (Mueller et al., 2018). This study found associations between excessive expansion or volume loss and time between MRI and SUDEP in srois covering structures involved in autonomic control at several brainstem levels. However, testing which combination of srois explained most of the variability identified srois in the upper (dorsal raphe) and lower brainstem (medulla oblongata). The findings in the medulla oblongata were consistent with the findings of an autopsy study (Patodia et al., 2018) in SUDEP patients which suggested that the lower brainstem abnormalities might be more important for SUDEP risk than upper brainstem abnormalities and that subdividing the brainstem in this way might allow to gain some additional insights into this question.

2.3.2. Characterization of the pattern of brain/brainstem volume loss by graph analysis: PSI approach

In order to investigate how the mean age-corrected gray matter z-score in one region is related to that of the other 450 Gy matter regions of interest (sroi) (380 cortical/subcortical AICHA regions, 71 brainstem cROIs) the so-called profile similarity index (PSI) was calculated The PSI between sroi x and sroi y is defined as follows:

$$\text{rawPSI} = (\text{sroi A} - \text{mean}_{\text{sroi}})/\text{abs}((\text{sroi x} - \text{mean}_{\text{sroi}}) - (\text{sroi y} - \text{mean}_{\text{sroi}}))$$

sroi A is either sroi x or sroi y whichever is larger, $\text{mean}_{\text{sroi,}}$ mean over all 451 srois, abs is absolute.

The rawPSI is calculated for each and every combination between two srois resulting in a 451 × 451 PSI matrix. The rawPSI values exceeding the 95 percentile of all PSI values in the map are replaced by

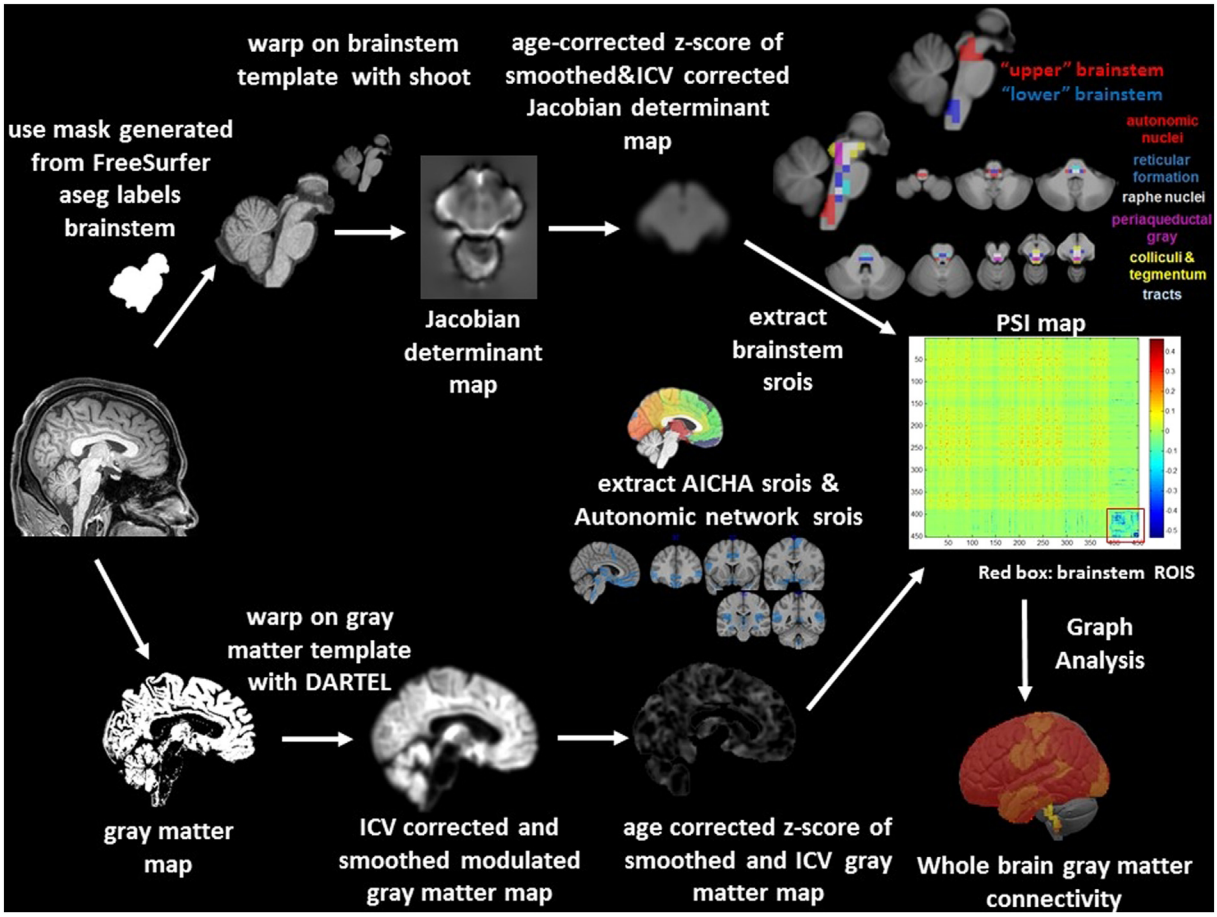

Fig. 1. Image processing of the structural data. The upper panel shows the processing steps for the calculation of the brainstem gray matter connectivity, the lower panel shows the processing steps for the calculation of the cortical/subcortical connectivity. The resulting maps (Jacobian determinant map for brainstem and modulated gray matter map for cortical/subcortical brain) are normalized and corrected for age effects by converting them into age corrected z-scores that allow to combine the information from the two regions for the calculation of the profile similarity index map (PSI). The red box on the PSI map indicates brainstem rois. Please see Methods section in the text body for a detailed description. ICV, intracranial volume, srois, regions of interest for structural imaging.

the PSI value at the 95 percentile to remove outliers caused by a difference of 0 or very small differences between sroi x and sroi y. The rawPSI map is then converted into a the final PSI map by multiplying it with a normalization term n defined as $n = 1/$(range of all raw PSI in map). A negative PSI indicates a gray matter decrease in this sroi relative to this subject's mean whole brain/brainstem gray matter and a positive PSI a gray matter increase in this sroi relative to this subject's mean whole brain/brainstem gray matter. It is assumed that the PSI map of an individual healthy control is determined by this person's individual anatomical features and thus that the PSI maps of the control group capture the common anatomical brain/brainstem variants. A pathological process within the region covered by the 451 srois will introduce additional srois with relative gray matter decrease or increase that will change the appearance of the resulting PSI map compared to those of the control group. Graph theory is used to summarize the pattern of relative gray matter decrease/increase captured by each subject's PSI map. The routines provided by the Brain Connectivity Toolbox (https://sites.google.com/site/bctnet) and in particular the weight conserving measure "strength", was used for this purpose (Rubinov and Sporns, 2011). Weight conserving measures have the advantage that they can be applied to fully connected networks, i.e., it is not necessary to define an arbitrary threshold to generate the type of sparse network required by the more commonly used non weighted equivalent degree. Strength is defined as the sum of weights of links connected to a sroi. A sroi has a high strength if it has experienced a similar degree of relative gray matter decrease or increase as the majority of the other srois and a low strength if there are only few other ROIs with similar relative gray matter decrease/increase. A brain and/or brainstem with gray matter loss due to a more or less focal pathological process will have a different strength profile than a healthy brainstem or brain. Finally, the BCT strength algorithm distinguishes between positive and negative strength. In the context of the PSI map, the negative strength of a sroi provides a measure of relative gray matter decrease of this sroi compared to other srois and the positive strength a measure for relative gray matter increase. Negative strength was chosen for the analysis since the focus of this study is on volume decrease.

2.3.3. Definition of gray matter connectivity networks of interest

Sroi brain gray matter connectivity is the negative strength of one of the 451 sroi calculated from its PSIs with the other 450 srois. Global brain gray matter connectivity is calculated as the average negative strength of these 451 srois. Sroi brainstem-brain gray matter connectivity is the negative strength of one of the 71 brainstem srois calculated from its PSIs with the other 450 srois. Global brainstem-brain gray matter connectivity is calculated as the average negative strength of each of the 71 brainstem srois brainstem gray matter connectivity. Upper and lower brainstem-brain gray matter connectivity and global upper and lower brainstem connectivity are the equivalents of brainstem-brain gray connectivity for the 16 upper and 11 lower brainstem srois. Sroi autonomic gray matter connectivity is the negative strength of one autonomic sroi calculated from its PSIs with the other 82

autonomic srois in regions known to be involved in autonomic control, i.e., posterior and anterior dorsal insula, hippocampus, amygdala, subgenual, mid and posterior cingulate, medial pregenual prefrontal and orbito-frontal cortex, orbital operculum angular and supramarginal cortex, hypothalamus/accumbens and autonomic brainstem regions (cf Figure, Macefield and Henderson, 2016, Beissner et al., 2013, Lacuey et al., 2016, Lacuey et al., 2017 and Lacuey et al., 2018, Edlow et al., 2016, Faull and Pattinson, 2017). Autonomic gray matter connectivity is calculated as the average negative strength of these 83 srois.

2.4. Functional imaging

2.4.1. Pre-processing

The first 10 time frames were discarded to allow the MRI signal to achieve T1 equilibrium. The remaining 230 timeframes/subject underwent slice time correction, motion correction and realignment onto a mean EPI image in the T1 space, spatial normalization using the transformation matrices generated during the warping of the gray matter maps onto the gray matter template with re-sampling to a 1.5 × 1.5 × 1.5 mm resolution. Framewise displacement (Power et al., 2012) was used to assess the motion during the exam. Conn 17f (www.nitrec.org/projects/conn/, Whitfield-Gabrieli and Nieto-Castanon, 2012) a SPM based toolbox for task and task-free fMRI analysis was used for further processing including linear detrending and band pass filtering (0.015–0.09 Hz) with simultaneous denoising. The latter included the aCompCorr routine to reduce the effects of physiological noise (eroded white (wo brainstem and diencephalon) and csf maps, 5 components each and motion regression (6 affine motion parameters and 6 first order temporal derivatives). In addition to that, ART as implemented in the conn preprocessing was used to identify timeframes with motion exceeding a movement threshold of 0.9 mm which ensures that conn disregards these timeframes during the denoising procedure but leaves the original time series intact. No global signal removal was performed since this is known to falsely increase anticorrelations between time series (Murphy et al., 2014). The AICHA atlas was used to extract the denoised mean time series from cortical and subcortical regions. A grid system of 16 14x14x14 voxel cubic ROIs was overlaid on the brainstem encompassing regions containing structural srois in the lower and mid pons, the ponto-mesencephalic junction and the mesencephalon and the denoised mean time series extracted and combined with the time series from the cortical/subcortical regions for the calculation of the functional connectivity of a total of 398 functional cortical/subcortical and brainstem regions of interest (frois). The functional brainstem rois were chosen bigger than the structural brainstem rois to account for the lower resolution of the EPI sequence (cf Fig. 2a).

2.4.2. Dynamic analysis

A sliding windows approach was used to explore temporal variations of functional connectivity. Based on observations that robust estimations of the functional connectivity without loss of potentially interesting fluctuations are possible with window sizes around 30–60 s (Hutchison et al.2013), a window with the size of 60 s (30 timeframes) that was advanced with increments of one TR along the artifact corrected time series was chosen resulting in 6965 windows for all 19 subjects (7 controls, 12 FE) that were converted into 6965 correlation matrices using Pearson correlation (cf Fig. 2b).

Graph analysis was used to describe the interactions between the different frois in each window (cf. Fig. 2c). The positive (pos) strength outputs for each window were combined to obtain a map showing the fluctuations of pos strength over the acquisition time for each froi for each subject and then concatenated across subjects to obtain population maps of pos strength for each froi (Fig. 2d). The positive strength of each froi in each window of this population map were converted into z-scores using mean and standard deviation of the froi strength of the 7 control subjects with the following formula: strength z-score of froi x in window n = strength of froi x in window n – mean of strength of froi x from all windows in controls/standard deviation of strength of froi x from all windows in controls. The thus calculated froi z-scores/window were averaged over 7 “large regions” (left and right anterior region (medial and lateral prefrontal and insular cortex), posterior region (parietal and occipital lobe, thalamus, caudate, pallidum, putamen), temporal region (lateral and medial temporal including hippocampus and amygdala) and brainstem) to obtain the average positive strength z-scores for each of these “large regions” for each window in each subject (Fig. 2e.). Hierarchical cluster analysis (Ward's minimum variance methods with the cubic clustering criterion to identify optimal cluster number) was used to identify different clusters or activity states based on their “large region” positive strength profiles in FE and controls (optimal cluster number = 22, please see Fig. 2f). The output generated by ART was used to identify windows with motion outliers and to calculate the % of motion outliers for each cluster. > 20% of the windows in clusters 14 and 16–22 were identified as motion outliers and therefore these clusters were considered to represent “motion clusters” and not further evaluated. This step also eliminated windows that despite not meeting the ART threshold for motion outliers themselves had a similar graph analytical profile as windows that did meet that threshold and were therefore likely to be affected by subthreshold motion (Fig. 2g.). All other clusters or activity states had < 15% of motion outliers (range 12.2%- < 1%) and were fully evaluated after excluding all motion outlier windows (Fig. 2h). Eliminating windows with excessive motion results in a more rigorous elimination of motion artifacts than just eliminating the motion affected timeframe alone because it also eliminates timeframes with subthreshold motion that usually accompany timeframes with suprathreshold motion. FWD was used to obtain a measure of remaining motion. The percentage of motion affected windows removed by this procedure was higher ($p < .02$) in patients (mean (SD): 13.4 (3.6)) than in controls (mean (SD): 8.8 (1.8)). The mean FWD/window after the removal of the motion affected windows was not different between the two groups (patients vs. controls: mean FWD/ window (SD): 0.26 (0.07) vs. 0.24 (0.08), $p > .05$) making it unlikely that potential group differences were driven by motion artifacts.

The duration of each of the 14 remaining activity states in a subject was calculated as the percentage of non-motion affected windows assigned to this activity state by the cluster analysis.

2.4.3. Definition of functional connectivity networks of interest

Froi brain functional connectivity is the z-score of the positive strength of one froi calculated from its correlations with the other 397 srois in this window. Global brain functional connectivity is calculated as the average z-score of the strengths of these 398 frois in this window. Froi brainstem-brain functional connectivity is the z-score of positive strength of one brainstem froi calculated from its correlations with the other 397 frois in this window. Global brainstem-brain functional connectivity is calculated as the average z-score of the positive strengths of the 16 brainstem frois with each of the other 397 frois in this window. Froi autonomic functional connectivity is the z-score of the positive strength of one autonomic froi calculated from its correlation with the other 43 autonomic frois in regions known to be involved in autonomic control, i.e., posterior and anterior dorsal insula, hippocampus, amygdala, subgenual, mid and posterior cingulate, medial pregenual prefrontal and orbito-frontal cortex, orbital operculum angular and supramarginal cortex, hypothalamus/accumbens and autonomic brainstem regions. Autonomic functional connectivity is calculated as the average z-score of the strengths of these 44 frois in this window.

To characterize the behavior of these subnetworks during each of the 15 activity states in an individual control or FE, the average positive functional subnetwork connectivity strength from all the windows assigned to an activity state weighted by the duration of this activity state in this subject was calculated.

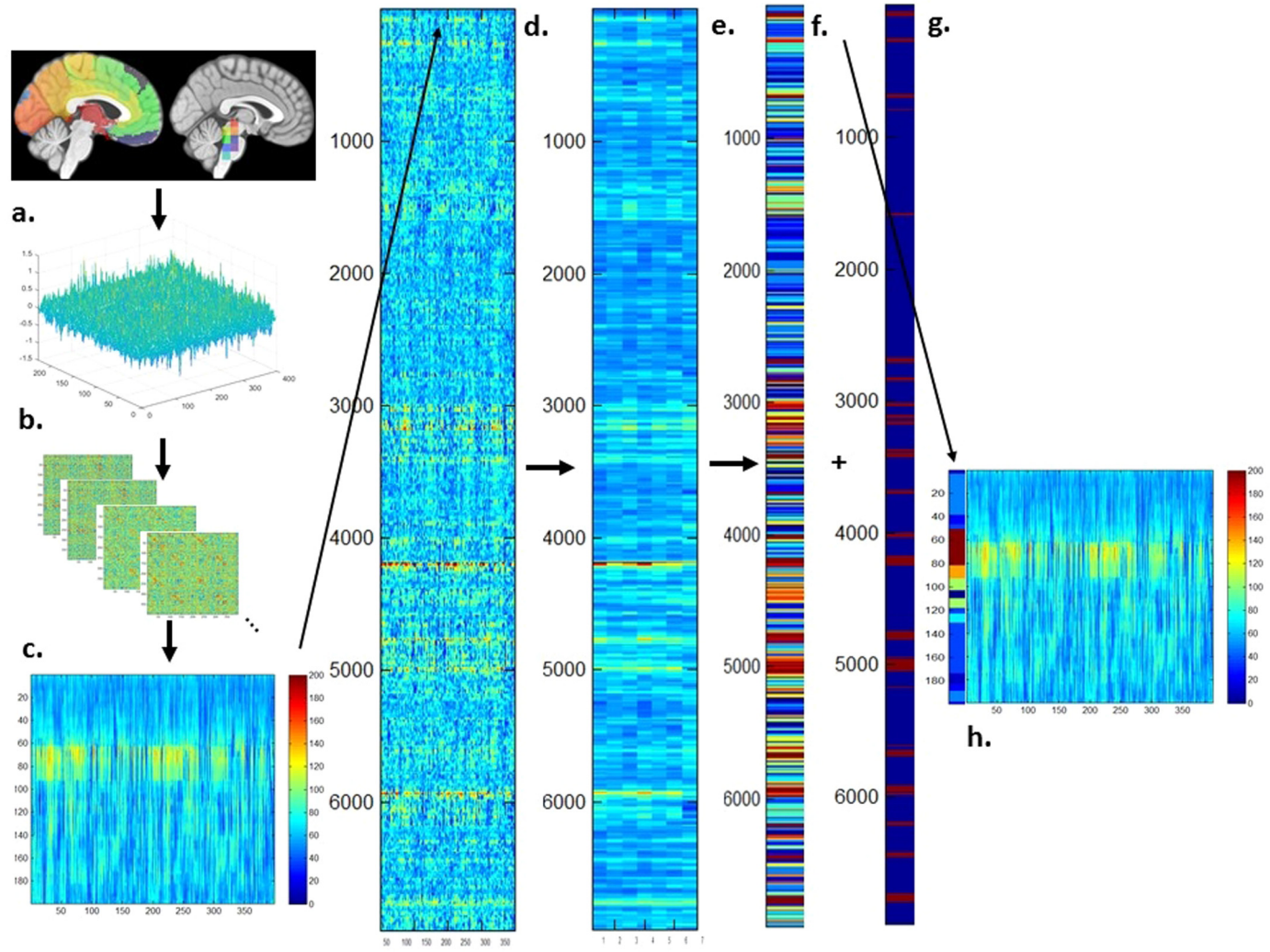

Fig. 2. Overview of the processing steps of the dynamic functional analysis. a. Cortical and subcortical AICHA parcellation and functional regions of interest (froi) in the brainstem. b. BOLD signals and correlation matrices extracted from one session. c. Positive strength map of a control subject. d. Concatenated positive strength maps from all 19 subjects with fMRI. e. "Large region positive strength z-scores map" that was used as input for the hierarchical cluster analysis. f. Cluster map, i.e., color-coded cluster assignment of each window, and g. ART output with windows flagged as motion outliers (red) on the right. h. Positive strength map with color coded cluster assignments on the left side, dark red indicates windows assigned to "motion clusters". Please see Methods section in the text body for a detailed description.

2.5. Statistics

One sided Kruskal-Wallis tests were used for group comparisons and Spearman rank tests were used to test for associations between HRV and structural and functional connectivity. False discovery rate (FDR) at 0.05 was used to correct for multiple comparisons.

3. Results

3.1. Structural

3.1.1. Group comparisons

Table 2 summarizes the global gray matter z-scores and connectivity differences between FE and controls. The comparison of the age-adjusted z-scores at the sroi level identified srois with volume loss in the region of the inferior colliculi and right inferior temporal gyrus in FE compared to controls ($p < .05$, FDR). None of the connectivity differences at the sroi level survived FDR correction when comparing, brainstem-brain connectivity, lower and upper brainstem-brain connectivity, and brainstem-cortical-autonomic network between controls and FE.

3.1.2. Associations between gray matter connectivity and HRV

Epilepsy patients had a lower heart rate adjusted HRV than controls (−0.176 (1.014) vs. 0.318 (0.941)) but the difference did not reach significance. Table 2 summarizes global gray matter connectivity HRV associations. When connections between all brainstem srois with cortical and subcortical srois in the rest of the brain were considered, impaired HRV was correlated with reduced gray matter connectivity between brainstem and right hippocampus/parahippocampus in controls ($p < .05$, FDR) and between brainstem and right parietal cortex, lingual gyrus, left hippocampus/amygdala, parahippocampus, temporal pole, septum and bilateral anterior thalamus in FE ($p < .05$, FDR) (cf. Fig. 3). None of the gray matter connectivity HRV associations in the control group survived FDR correction when only reduced gray matter connectivity strength between srois in the lower brainstem and other brainstem regions/subcortical/cortical gray matter regions was investigated. In FE, reduced gray matter connectivity between lower brainstem with left amygdala, left temporal pole and with autonomic srois in the pons was associated with impaired HRV. When HRV/Gy matter connectivity strength associations between upper brainstem srois with the rest of the brain were investigated, none of the associations between impaired HRV and reduced gray matter connectivity

Table 2
Summary structural z-scores and connectivities.

Measure	Control Mean (SD)	LRE Mean (SD)
Global brain gray matter z-score	−0.14 (0.33)	−0.25 (0.42)
Global brainstem z-score	0.10 (1.00)	−0.30 (1.25)
Global lower brainstem z-score	0.33 (1.13)	−0.25(1.07)
Global upper brainstem z-score	−0.03 (1.04)	−0.25 (1.49)
Autonomic network z-score	0.01 (0.68)	−0.30 (0.92)
Global brainstem - brain gray matter connectivity	6.0 (5.70)	7.2 (6.1)
Lower global brainstem - brain gray matter connectivity	5.3 (6.4)	6.4 (5.7)
Upper global brainstem - brain gray matter connectivity	6.3 (5.6)	7.8 (6.5)
autonomic network gray matter connectivity	1.5 (1.43)	2.0 (2.0)

	Correlation with HRV in Controls	Correlation with HRV in LRE
Global brainstem - brain gray matter connectivity	−0.77*	−0.64*
Lower global brainstem - brain gray matter connectivity	−0.66 *	−0.69 *
Upper global brainstem - brain gray matter connectivity	−0.72*	−0.60*
Autonomic network gray matter connectivity	−0.76 *	−0.69*

z-score, age corrected z-score, (SD), standard deviation, HRV heart rate variability, please see text body for definition of “upper” and “lower” brainstem.

strength survived FDR correction in the control group. In FE, significant HRV/upper brainstem gray matter connectivity strength associations were found in the left hippocampus, left medial prefrontal cortex, right lingual gyrus, precuneus and anterior thalamus, and in pontine and medullo-pontine autonomic brainstem srois. When the criteria for significance were relaxed ($p < .005$) additional gray matter connectivity strength/HRV associations were revealed. In FE these associations were found in the bilateral mesial temporal region, thalamus, medial prefrontal and upper brainstem in all investigated network types. In controls, additional HRV/Gy matter connectivity associations were found orbitofrontal, dorso-lateral and medial prefrontal, putamen, hippocampus, thalamus and brainstem (cf. Fig. 3).

When the analysis was restricted to the autonomic network, reduced dorsal raphe gray matter connectivity was correlated with impaired HRV in controls ($p < .05$, FDR). In FE significant correlations between impaired HRV and reduced autonomic network gray matter connectivity were found in the upper (region of periaqueductal gray, dorsal raphe, formatio reticularis) and lower brainstem (region of dorsal motor nucleus of the vagus nerve, nucleus ambiguus, formatio reticularis of the pons and medulla) and also in the left posterior

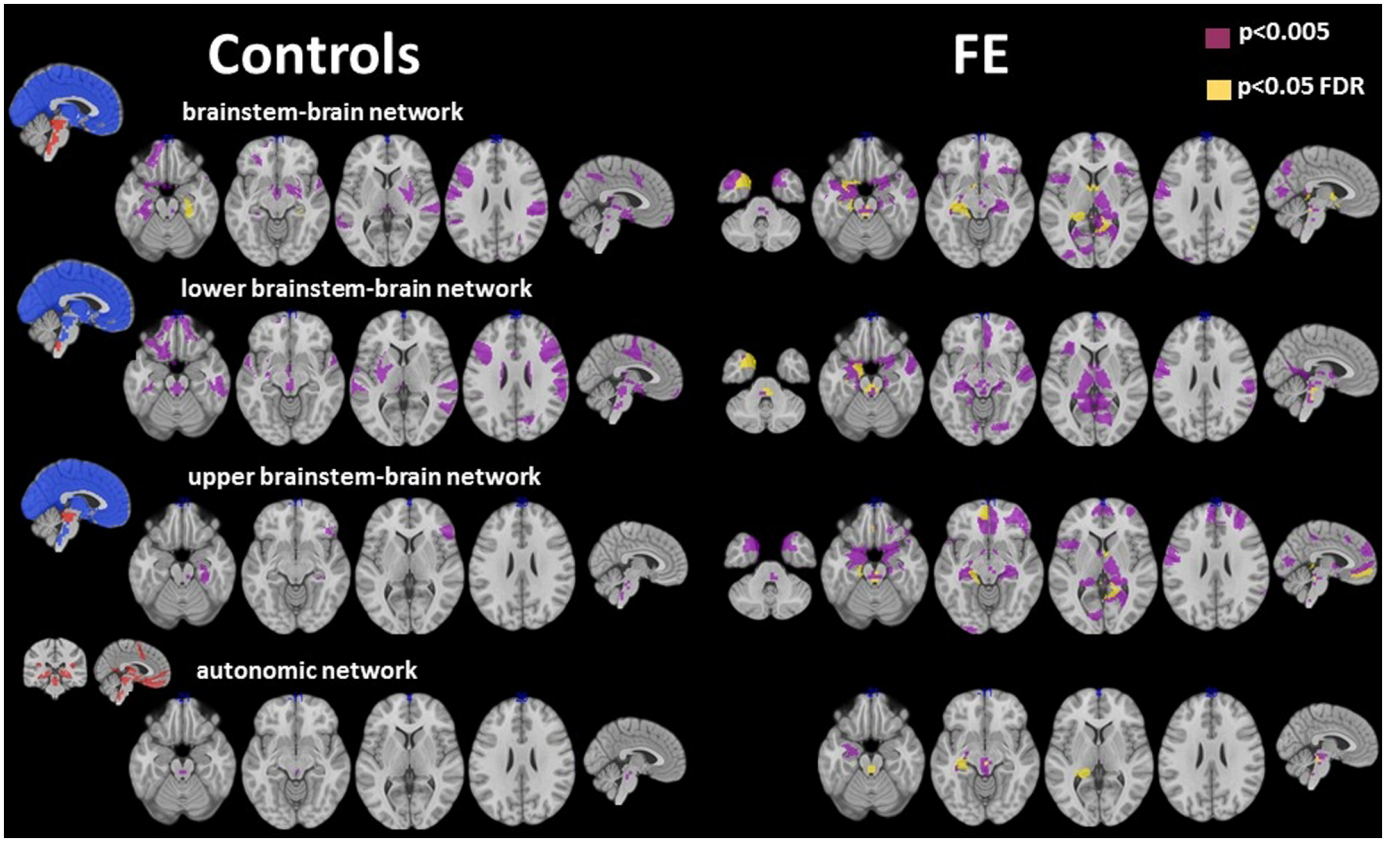

Fig. 3. Overview of rois with gray matter connectivity with significant HRV associations. Left findings in controls, right findings in FE. Blue, srois for which HRV/ Gy matter connectivity is calculated based on PSI values with red srois. Red, srois for which HRV/Gy matter connectivity is calculated based on PSI values with other red srois and blue srois.

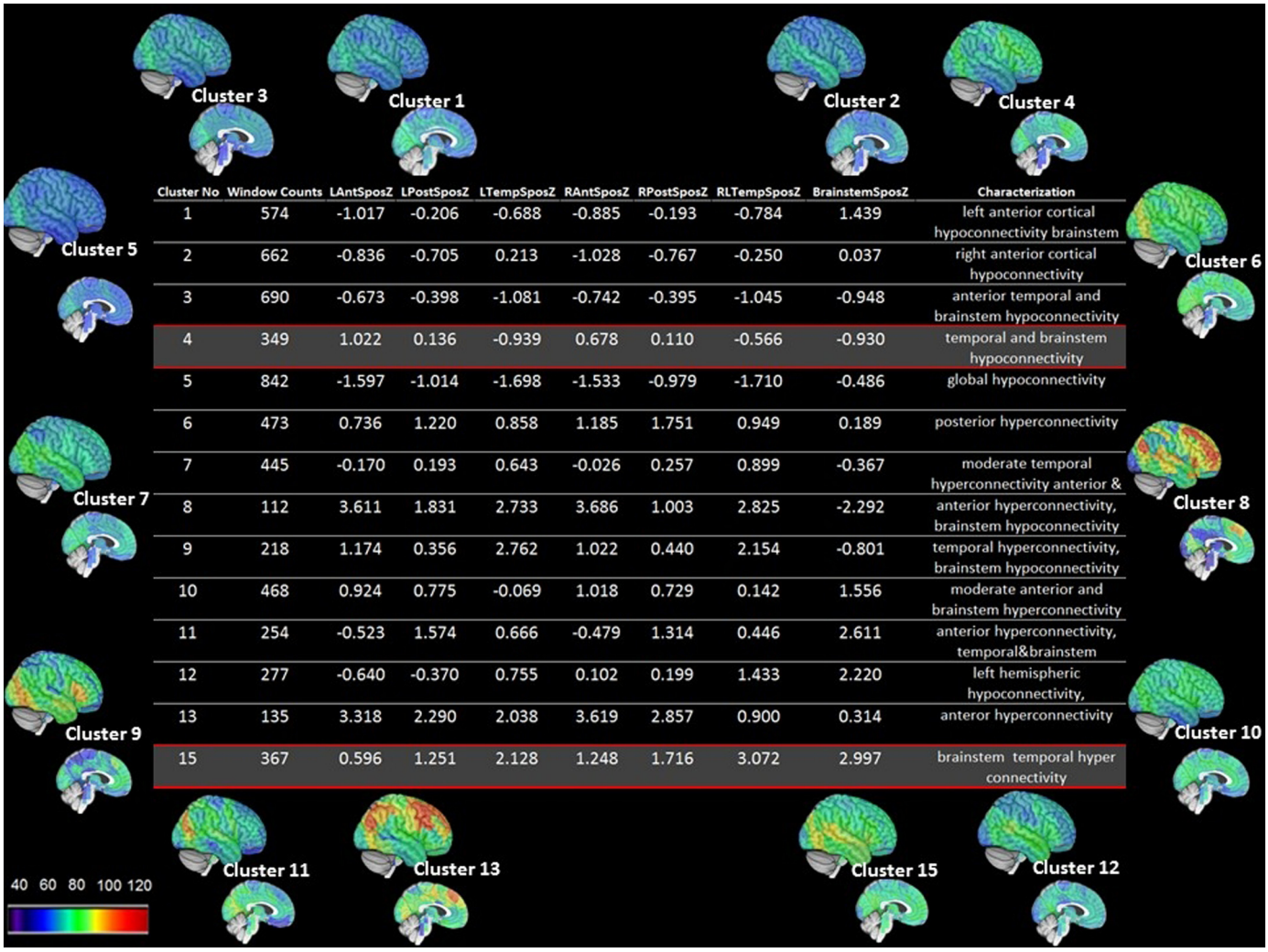

Cluster No	Window Counts	LAntSposZ	LPostSposZ	LTempSposZ	RAntSposZ	RPostSposZ	RLTempSposZ	BrainstemSposZ	Characterization
1	574	-1.017	-0.206	-0.688	-0.885	-0.193	-0.784	1.439	left anterior cortical hypoconnectivity brainstem
2	662	-0.836	-0.705	0.213	-1.028	-0.767	-0.250	0.037	right anterior cortical hypoconnectivity
3	690	-0.673	-0.398	-1.081	-0.742	-0.395	-1.045	-0.948	anterior temporal and brainstem hypoconnectivity
4	349	1.022	0.136	-0.939	0.678	0.110	-0.566	-0.930	temporal and brainstem hypoconnectivity
5	842	-1.597	-1.014	-1.698	-1.533	-0.979	-1.710	-0.486	global hypoconnectivity
6	473	0.736	1.220	0.858	1.185	1.751	0.949	0.189	posterior hyperconnectivity
7	445	-0.170	0.193	0.643	-0.026	0.257	0.899	-0.367	moderate temporal hyperconnectivity anterior &
8	112	3.611	1.831	2.733	3.686	1.003	2.825	-2.292	anterior hyperconnectivity, brainstem hypoconnectivity
9	218	1.174	0.356	2.762	1.022	0.440	2.154	-0.801	temporal hyperconnectivity, brainstem hypoconnectivity
10	468	0.924	0.775	-0.069	1.018	0.729	0.142	1.556	moderate anterior and brainstem hyperconnectivity
11	254	-0.523	1.574	0.666	-0.479	1.314	0.446	2.611	anterior hyperconnectivity, temporal&brainstem
12	277	-0.640	-0.370	0.755	0.102	0.199	1.433	2.220	left hemispheric hypoconnectivity,
13	135	3.318	2.290	2.038	3.619	2.857	0.900	0.314	anteror hyperconnectivity
15	367	0.596	1.251	2.128	1.248	1.716	3.072	2.997	brainstem temporal hyper connectivity

Fig. 4. Characterization of the 14 non-motion clusters or activity states. LAntSposZ, averaged pos strength z-scores over left anterior hemisphere, LPosSposZ, averaged pos strength z-scores over left posterior hemisphere, LTempSposZ, averaged pos strength z-scores over left temporal lobe, RAntSposZ, averaged pos strength z-scores over right anterior hemisphere, RPosSposZ, averaged pos strength z-scores over right posterior hemisphere, RTempSposZ, averaged pos strength z-scores over right temporal lobe, BrainstemSposZ, averaged pos strength z-scores over brainstem. Anterior region includes functional rois (frois) in medial and lateral prefrontal and insular cortex, posterior region includes frois in the parietal and occipital lobes thalamus, caudate, pallidum, putamen, temporal region includes frois in lateral and medial temporal including hippocampus and amygdala) and brainstem includes all brainstem frois.

hippocampus ($p < .05$, FDR).

The main findings reported here for 19 FE were unchanged when the analysis was restricted to the 12 FE with task-free fMRI.

3.2. Functional dynamic analysis

Not counting clusters affected by motion, the cluster analysis identified 14 activity states. Please see Fig. 4 for characterization. The number of activity states displayed per subject ranged between 6 and 13 (controls: mean (SD) 10.7 (2.2), FE: mean (SD): 9.6 (2.0), p = ns). Functional brainstem-cortex connectivity was significantly correlated with HRV in two of these activity states.

Activity state 4 (Fig. 5 upper panel): The strength profile of this state was characterized by an intermediate overall positive strength that was slightly higher over the anterior brain regions and slightly reduced in orbito-frontal and temporal regions and brainstem. The latter indicates a tendency for de-synchronization of the activity of orbito-frontal, temporal and brainstem with that of the rest of the brain. The functional brainstem-cortex connectivity strength during activity state 4 was positively correlated with HRV ($r = 0.57$, $p = .03$). The same was also true for functional connectivity strength within the autonomic network ($r = 0.55$, $p = 0.04$). Given the association of HRV with autonomic gray matter connectivity strength and with brainstem-brain gray matter connectivity strength reported in the previous section, the effect of the structural abnormality on the HRV functional connectivity association was investigated. Structural brainstem-brain gray matter connectivity and functional brainstem-brain connectivity together explained 63% ($p = .007$) of the HRV variability in this population and structural autonomic network connectivity and functional autonomic connectivity together explained 85% ($p = .0002$). Brainstem-brain gray matter connectivity (whole brainstem, lower and upper brainstem) did not correlate with functional brainstem-brain connectivity nor did gray matter autonomic connectivity correlate with the functional autonomic network connectivity. The activity state was observed in 71% of the controls and 58% of the FE. The time during which it could be observed in subjects showing this activity was not different between controls and FE (controls: mean 6.7 (8.4) percent of the time, FE: mean 4.2 (4.4) percent of the time.

Activity state 15 (Fig. 5 lower panel): The strength profile of this state was characterized by a generally increased positive strength that was most pronounced over the hippocampi, superior temporal and frontal opercular regions, insula and the brainstem. Restricting the

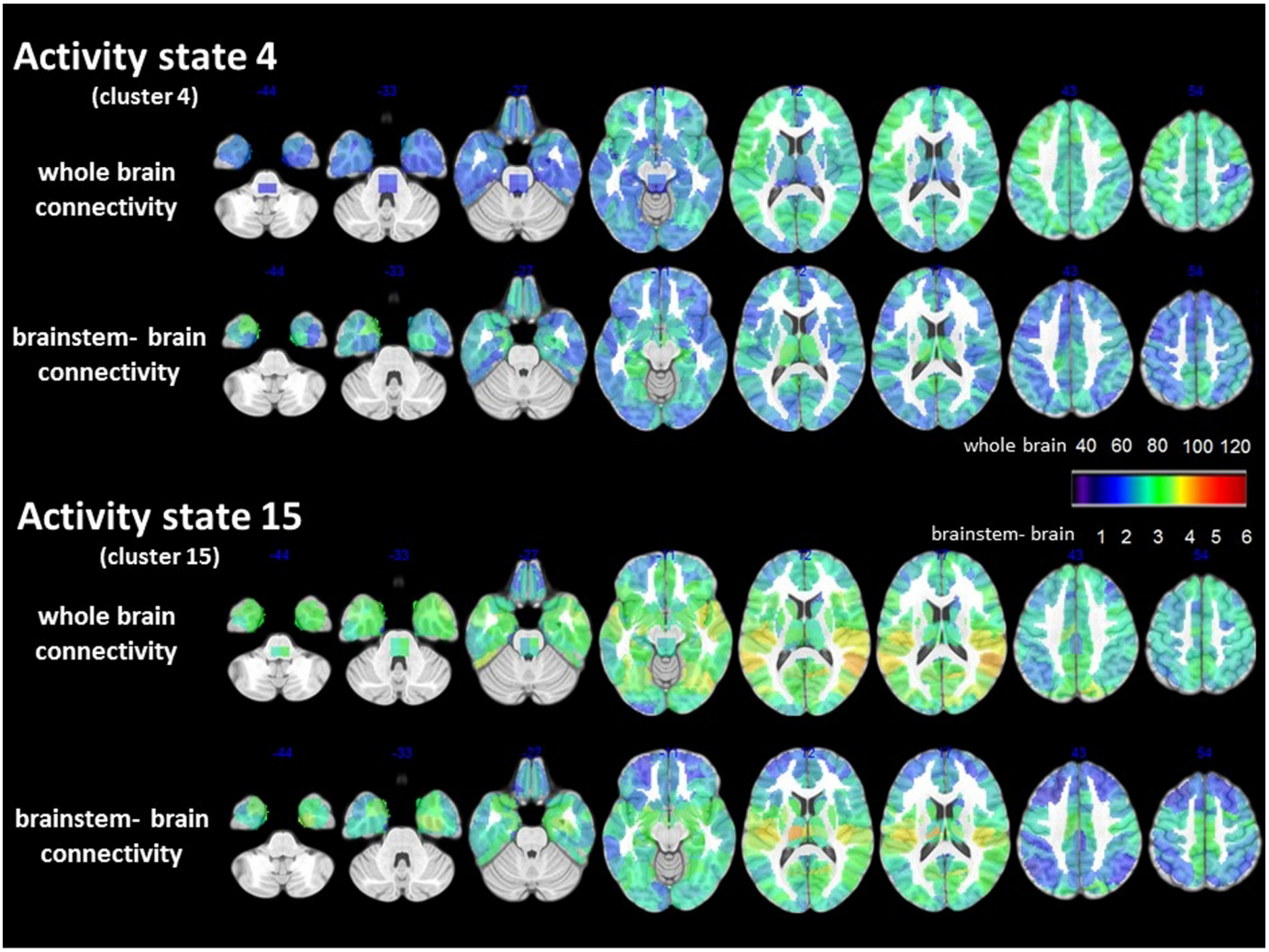

Fig. 5. Details of activity state 4 and 15. The upper panel depicts the whole brain positive strength pattern or connectivity during this state the lower panel the brainstem-brain connectivity pattern, i.e. positive strength calculated based on connections between brainstem frois with cortical and subcortical frois but without connections only between subcortical and cortical frois. Please see intensity scaling. During activity state 4 the whole brain connectivity strength of brainstem and bilateral, inferior, lateral temporal lobes, orbitofrontal and thalamus regions is comparatively low compared to the rest of the brain but pronounced when the connectivity is restricted to brainstem-brain connections indicating a heightened degree of synchronization between these regions and a decreased degree of synchronization with other cortical/subcortical region Activity state 15 is the state with the highest brainstem connectivity and whole brain connectivity is characterized by strong brainstem superior temporal, insula connections. This pattern persists when only brainstem-brain connectivity is considered which indicates that the brainstem activity influences the activity in these regions.

connectivity analyses to the frois of the left or the right temporal lobe structures showed only moderate connectivity increases in FE within these structures even when taking the focus localization into account (left FE: mean z-score left: 0.78 (0.49), right: 0.78 (0.39); right FE: mean z-score left: 0.11 (0.47), right: 0.49 (0.36); bilateral/no-lateralized FE: mean z-score left: −0.01 (0.33), right: 0.59 (0.29)). The same was true for within brainstem connectivity (left FE:1.1 (0.63), right FE: 0.21(0.5); bilateral/non-localized FE: −0.23 (0.40)). This indicates that not activity within the brainstem or within temporal lobe structures was driving the increased brainstem-brain activity during this state but an increased synchronization of the activity between these structures. The functional brainstem-brain connectivity strength during this state was negatively correlated with HRV ($r = -0.50$, $p = .03$) and explained 25% of the HRV variability. Functional brainstem-brain connectivity was positively correlated with reduced brainstem-brain gray matter connectivity ($r = 0.46$, $p = .04$) and with reduced lower brainstem-brain gray matter connectivity ($r = 0.49$, $p = .03$) but not with reduced upper brainstem-brain gray matter connectivity strength. Functional connectivity within the autonomic network during activity state 15 did not correlate with HRV. Activity state 15 was observed in 57% of the controls and 92% of the FE. The duration of activity state 15 was significantly longer in FE than in controls (controls with activity state 15 activity: mean 2.0 (3.8) percent of the time, FE with activity state 15 activity: mean 9.4 (7.1) percent of the time).

4. Discussion

The study had the following two major findings: 1. FE showed HRV/Gy matter connectivity associations in the upper brainstem, mesial-temporal, temporo-polar, mesial prefrontal and thalamic regions, i.e., regions known to be involved in autonomic control and to be affected by volume losses in FE. The network type (whole brainstem-brain, upper, lower brainstem-brain seeds) had no influence on the observed pattern. These findings suggest that impaired autonomic control in FE is more likely to be determined by the accumulation of gray matter damage throughout structures involved in autonomic control or "network damage" than by damage to one or a few "critical" structures, e.g. amygdala or brainstem (Macefield and Henderson, 2016). 2. Dynamic

task-free fMRI analysis identified two activity states during which the expression of the brainstem-brain interactions was significantly associated with HRV. The two states however differed not only regarding the nature of their association with HRV but also on how their own expression was influenced by brainstem-brain or autonomic gray matter connectivity.

Taken together, the findings suggest that interictal HRV dysfunction in FE is associated with structural abnormalities in brain regions involved in autonomic control at the brainstem level but also at the cortical/subcortical level. These structural abnormalities affect not only the brainstem's ability to initiate/maintain physiological brain activity states involved in autonomic control but also facilitate the appearance of activity states that may disrupt autonomic control. The latter type could result in a heightened risk for SUDEP if the structural abnormalities worsen over time and these states get longer and more severe.

The first major finding was the consistent association between HRV and gray matter connectivity with mostly upper brainstem srois, i.e., mesencephalon, upper pons, and hippocampus, amygdala and temporal pole srois in FE. The association HRV with upper brainstem gray matter connectivity was expected. The brainstem srois had been chosen in regions known to be associated with autonomic control and so this finding can be considered proof that the PSI approach allows to detect biologically meaningful information. The association between HRV and hippocampus gray matter connectivity not only reflects the role of the hippocampus in autonomic control (Napadow et al., 2008) but also the strong connections between hippocampus and brainstem (Commons, 2016; Hornung, 2003; Coulombe et al., 2016). This is supported by the finding in controls who had the same although weaker associations between HRV and hippocampus/brainstem gray matter connectivity than FE. Relaxing the criteria for significance ($p < .005$, no FDR correction) in FE revealed additional significant associations between HRV and impaired gray matter connectivity of the lower brainstem, thalamus, mesial and dorso-lateral prefrontal cortex, i.e., other regions known to be involved in autonomic control (Beissner et al., 2013; Macefield and Henderson, 2016), and also of the lateral temporal and medial parietal lobe. The subcortical/cortical connectivity patterns of these associations were quite similar regardless of brainstem srois used as seeds (whole, upper, lower) and their distribution corresponded to the typical gray matter atrophy pattern seen in FE with temporal lobe onset, i.e., mesial temporal, temporal pole, thalamus, mesial prefrontal, insula (Whelan et al., 2018). This suggests that gray matter volume losses driving altered gray matter connectivity in FE could be caused by the same mechanisms, i.e., excitotoxic effects of epileptogenic activity in the focus and regions involved in seizure spread that accumulate in autonomic brain regions and impair autonomic control. As a consequence, autonomic regions with strong connections to the hippocampus/mesial temporal lobe, e.g. upper brainstem, thalamus, etc. are most likely to be affected and the combined damage in these regions will determine the degree of autonomic impairment. Taken together, the structural findings suggest that impaired autonomic control in FE is more likely to be determined by the accumulation of gray matter damage throughout the autonomic network or “network damage” than by damage to one or few “critical” structures, e.g. amygdala or brainstem. It must be emphasized though that this does not necessarily also apply to SUDEP risk for which abnormalities in the lower brainstem seem to play an important role (Patodia et al., 2018; Mueller et al., 2014; Mueller et al., 2018; Aiba and Noebels, 2015).

The second major finding was the identification of two brain activity states during which the brainstem brain connectivity strength was significantly correlated with HRV. Activity state 4 was found with the same frequency in controls and patients. The strength of its expression was positively correlated with HRV and this was also true when the analysis was restricted to regions known to be involved in autonomic control. The strength of the gray matter connectivity and strength of the functional connectivity within the autonomic network during this state together explained 80% of the variability of the HRV in the study population. Taken together, activity state 4 had all the characteristics of a state involved in maintaining normal autonomic function.

In contrast, activity state 15 had all the characteristics of a state interfering with the normal autonomic function. It appeared with a higher frequency in patients than in controls and the strength of its expression was negatively correlated with HRV. Although it was the state with the strongest functional brainstem-brain interactions, the within temporal lobe connectivity were only moderately increased. This makes it unlikely that these states were caused by an interictal epileptic discharge because epileptic activity spreading from the focus to the brainstem would be expected to be associated with a high within temporal lobe connectivity state in the epileptic temporal lobe (Mueller, 2018). Furthermore, reduced brainstem-brain gray matter connectivity and in particular reduced lower brainstem-brain gray matter connectivity was positively correlated with the strength of the expression of activity state 15 suggesting that the loss of afferent and efferent projections between lower brainstem, i.e., the region that has been associated with SUDEP (Mueller et al., 2018) and cortex/subcortical structures plays a role in the appearance of this state. Interestingly, the kind of abnormalities of the serotoninergic, somatostatin/galanin system in the ventrolateral medulla of SUDEP cases described by Patodia et al. (2018) have also been shown to enhance interictal cortical excitability in animal models (Cui et al., 2013; Guedes et al., 2017). Based on these observations, it is conceivable that further impairment of the brainstem-brain gray matter connectivity for example due to the excitotoxic damage of insufficiently controlled seizures could increase the frequency and severity of activity state 15 and thereby also enhance its ability to fatally destabilize autonomic control.

HRV and measures derived from it have been proposed as a potential biomarker for SUDEP risk (Myers et al., 2018; Baysal-Kirac et al., 2017; Novak et al., 2015). The findings of this study suggest that functional and structural connectivity abnormalities associated with FE with temporal origin impair the interactions between brainstem and cortical/subcortical autonomic centers and thereby autonomic control in several and complex ways. If the assumption that HRV disturbances associated with damage to lower brainstem (Patodia et al., 2018; Mueller et al., 2018) are indeed more harmful than those for example associated with upper brainstem or amygdala damage can be corroborated then the finding of a reduced HRV in FE without information regarding the structural and functional abnormalities associated with it is could explain why some studies found it of limited value regarding SUDEP risk (Ryvlin et al., 2019).

This study has several limitations. 1. The study population was small and only a subset had functional imaging. The patient population was a convenience population, i.e., no attempts had been made to enrich it with patients with increased SUDEP risk. It is therefore not possible to assess the relationship of known SUDEP risk factors, e.g. presence of secondary generalized seizures, duration of epilepsy etc. with the imaging findings in this study. The findings of this study are therefore at best preliminary and need to be confirmed in a larger study that accounts for all these factors. 2. The MRI sequences used in this study were not optimized for brainstem imaging. The T1 weighted structural image does not depict brainstem structures of interest reliably making it necessary to use macroscopic landmarks nearby to identify their approximate location. The fMRI sequence was a standard whole brain EPI sequence that while covering a fair amount of the brainstem did not cover it to the same extent as the structural image. Although the two lower most frois extended into the upper medulla oblongata the coverage of that area was deemed insufficient for a meaningful subdivision into a lower and upper brainstem similarly as it was done with the structural data. 3. A single ECG trace from the EEG recordings before the MR exam was used for the HRV calculation. Although effective for the purpose of this study, it is not state of the art and more sophisticated ECG recordings would have offered additional insights. 4. As pointed out in the methods section, brainstem nuclei/regions involved in autonomic control are not distinguishable on a

standard T1 weighted image at 3 T. Therefore, macroscopic landmarks were used to identify brainstem regions of interest and to verify the accuracy of the roi placements in individual subjects. Roi shape was chosen in a way that ensured that the structure of interest was included and its size adapted to the image resolution. It cannot be excluded that the results would have been different if a dedicated multi-modality brainstem imaging protocol (Lambert et al., 2013) that allows to depict some details of the internal brainstem structure had been used.

Supplementary data to this article can be found online at https://doi.org/10.1016/j.nicl.2019.101888.

Funding

This work was supported by the National Institute of Health (U01NS090406-02 to AMG) and UCSF REAC grant and Epilepsy Foundation grant 325981 to SGM.

None of the authors has to declare a conflict of interest in relationship to this work.

References

Aiba, I., Noebels, J., 2015. Spreading depolarization in the brainstem mediates sudden cardiorespiratory arrest in mouse SUDEP models. Sci Trans Med 7 (282), 282ra46. https://doi.org/10.1126/scitranslmedaaa4050.

Ashburner, J., Friston, K.J., 2011. Diffeomorphic registration using geodesic shooting and Gauss-Newton optimization. Neuroimage 55, 954–967.

Baysal-Kirac, L., Serbest, N.G., Sahin, E., Dede, H.O., Gürses, C., Gökyigit, A., Bebek, N., Bilge, A.K., Baykan, B., 2017. Analysis of heart rate variability and risk factors for SUDEP in patients with drug-resistant epilepsy. Epilepsy Behav. 71, 60–64.

Beissner, F., Meissner, K., Bär, K.J., Napadow, V., 2013. The autonomic brain: an activation likelihood estimation meta-analysis for central processing of autonomic function. J. Neurosci. 33, 10503–10511.

Celada, P., Puig, M.V., Artigas, F., 2013. Serotonin modulation of cortical neurons and networks. Front. Integr. Neurosci. https://doi.org/10.3389/fnint.2013.00025.

Commons, K.G., 2016. Ascending serotonin neuron diversity under two umbrellas. Brain Struct. Funct. 22, 3347–3360.

Coulombe, M.A., Erpelding, N., Kucyi, A., Davis, K.D., 2016. Intrinsic functional connectivity of periaqueductal gray subregions in humans. Hum Brain Map 37, 1514–1530.

Cui, Y., Li, G.H., Yamada, H., Watanabe, Y., Kataoka, Y., 2013. Chronic degeneration of dorsal raphe serotoninergic neurons modulates cortical spreading depression: a possible pathophysiology of migraine. J. Neurosci. Res. 91, 737–744.

deGee, J.W., Colizoli, O., Kloosterman, N.A., Knapen, T., Nieeiwenhuis, S., Donner, T.H., 2017. Dynamic modulation of decision by brainstem arousal systems. eLife. https://doi.org/10.7554/eLife.23232.

Devinsky, O., Hesdorffer, D.C., Thurman, D.J., Lhatoo, S., Richerson, G., 2016. Sudden unexpected death in epilepsy: epidemiology, mechanisms and prevention. Lancet Neurol. 15, 1075–1088.

Dlouhy, B.J., Gehlbach, B.K., Kreple, C.J., Kawasaki, H., Oya, H., Buzza, C., Granner, M.A., Welsh, M.J., Howard, M.A., Wemmie, J.A., Richerson, G.B., 2015. Breathing inhibited when seizures spread to the amygdala and upon amygdala stimulation. J. Neurosci. 35, 10281–10289.

Edlow, B.L., MaNab, J.A., Witzel, T., Kinney, H.C., 2016. 2015. Structural connectome of the human central homeostatic network. Brain Connect 6, 187–200.

Faull, O.K., Pattinson, K.T.S., 2017. The cortical connectivity of the periaqueductal gray and the conditioned response to the threat of breathlessness. eLife. https://doi.org/10.7554/eLife.21749.001.

Guedes, R.C.A., Araujo, M.D.G.R., Vercosa, T.C., Bion, F.M., de Sa, A.L., Pereira, A., Abadie-Guedes, R., 2017. Evidence of an inverse correlation between serotoninergic activity and spreading depression propagation in the rat cortex. Brain Res. 1672, 29–34.

Harden, C., Tomson, T., Gloss, D., Buchhalter, J., CrossJH, Donner E., French, J.A., Hesdorffer, D.C., Smithson, W.H., Spitz, M.C., Walczak, T.S., Sander, J., Ryvlin, P., 2017. Practice guideline summary: sudden unexpected death in epilepsy incidence rates and risk factors. Neurology 88, 1674–1680.

Holt, R.L., Arehart, E., Hunanyan, A., Fainberg, N.A., Mikati, M.A., 2016. Pediatric sudden unexpected death in epilepsy: what have we learned from animal and human studies. Semin. Pediatr. Neurol. 23, 127–133.

Hornung, J.P., 2003. The human raphe nuclei and the serotoninergic system. J Chem Neu 26, 331–343.

Joliot, M., Jobard, G., Naveau, M., Delcroix, N., Petit, L., Zago, L., Crivello, F., Mellet, E., Mazoyer, B., Tzourio-Mazoyer, N., 2015. AICHA: an atlas of intrinsic connectivity of homotopic areas. J. Neurosci. Methods 254, 46–59.

Jones, L.A., Thomas, R.H., 2017. Sudden death in epilepsy: insights from the last 25 years. Seizure 44, 232–236.

Kommajosyula, S.P., Randalll, M.E., Brozoski, T.J., Odintsov, B.M., Faingold, C.L., 2017. Specific subcortical structures are activated during seizure-induced death in a model of sudden unexpected death in epilepsy (SUDEP): a manganese-enhanced magnetic resonance imaging study. Epilepsy Res. 135, 87–94.

Lacuey, N., Zonjy, B., Theeranaew, W., Loparo, K.A., Tatsuoka, C., Sahadevan, J., Lhatoo, S.D., 2016. Left insular damage, autonomic instability and sudden unexpected death in epilepsy. Epilepsy Behav. 55, 170–173.

Lacuey, N., Zonjy, B., Londono, L., Lhatoo, S.D., 2017. Amygdala and hippocampus are symptomatogenic zones for central apneic seizures. Neurology 88, 701–705.

Lacuey, N., Hampson, J.P., Theeranaew, W., Zonjy, Vithala A., Hupp, N.J., Loparo, K.A., Miller, J.P., Lhatoo, S.D., 2018. Cortical structures associated with human blood pressure control. JAMA Neurol 75, 194–202.

Lambert, C., Lutti, A., Helms, G., Frackowiak, R., Ashburner, J., 2013. Multiparametric brainstem segmentation using a modified multivariate mixture of Gaussians. Neuroimage Clinical 2, 684–694.

Lhatoo, S.D., Nei, M., Raghavan, M., Sperling, M., Zonjy, B., Lacuey, N., Devinsky, O., 2016. Non-seizure SUDEP, sudden unexpected death in epilepsy without preceding epileptic seizures. Epilepsia 57, 1161–1168.

Macefield, V.G., Henderson, L.A., 2016. Real-time imaging of cortical and subcortical sites of cardiovascular control: concurrent recordings of sympathetic nerve activity and fMRI in awake subjects. J. Neurophysiol. 116, 1199–1207.

Mueller, S.G., 2018. Amyloid causes intermittent network dysfunctions in cognitively intact older subjects. Brain Imaging Behav 2018. https://doi.org/10.1007/s11682-018-9869.

Mueller, S.G., Weiner, M.W., 2017. Amyloid causes intermittent network disruptions in cognitively intact older subjects: structural connectivity matters. Front. Aging Neurosci. https://doi.org/10.3389/fnagi.2017.00418.

Mueller, S.G., Bateman, L.M., Laxer, K.D., 2014. Evidence for brainstem network disruption in temporal lobe epilepsy and sudden unexplained death in epilepsy. Neuroimage Clin 5, 208–216.

Mueller, S.G., Nei, M., Bateman, L.M., Knowlton, R., Laxer, K.D., Friedman, D., Devinsky, O., Goldman, A.M., 2018. Brainstem network disruption: a pathway to sudden unexplained death in epilepsy? Hum. Brain Mapp. 39, 4820–4830.

Murphy, K., Birn, R.M., Handwerker, D.A., Jones, T.B., Bandettini, P.A., 2014. The Impact of Global Signal Regression on Resting State Correlations: Are Anticorrelated Networks Introduced? Neuroimage. vol. 44. pp. 893–905.

Myers, K.A., Bello-Espinosa, L.E., Symonds, J.D., Zuberi, S.M., Clegg, R., Sadleir, L.G., Buchhalter, J., Scheffer, I.E., 2018. Heart rate variability in epilepsy: a potential biomarker of sudden unexpected death in epilepsy. Epilepsia 59, 1372–1380.

Naidich, T.P., Duvernoy, H.M., Delman, B.N., Sorensen, A.G., Kollias, S.S., Haacke, E.M., 2009. Internal architecture of the brainstem with key axial section. In: Duvernoy's Atlas of the Human Brainstem,and Cerebellum. High-Field MRI: Surface Anatomy, Internal Structure, Vascularization and 3D Sectional Anatomy. Springer, Vienna, Austria, pp. 53–93.

Napadow, V., Dhond, R., Conti, G., Makris, N., Brown, E.N., Barbieri, R., 2008. Brain correlates of autonomic modulation: combining heart rate variability with fMRI. Neuroimage 42, 169–177.

Neves, R.M., van Keulen, S., Yang, M., Logothetis, N.K., Eschenko, O., 2018. Locus coeruleus phasic discharge is essential for stimulus induced-gamma oscillations in the prefrontal cortex. J. Neurophysiol. 119, 904–920.

N'Gouemo, P., Faingold, C.L., 2000. Phenytoin administration reveals a differential role of pontine reticular formation and periaqueductal gray neurons in generation of the convulsive behaviors of audiogenic seizures. Brain Res. 859, 311–317.

Novak JL, Miller PR, Markovic D, Meymandi SK, De Giorgio CM, 2015. Risk assessment for sudden death in epilepsy: the SUDEP-7 inventory. Front Neurol doi: https://doi.org/10.3289/fneur.2015.00252.

O'Brien, P.C., Dyck, P.J., 1995. Procedures for setting normal values. Neurology 45, 17–23.

Patodia, S., Somani, A., O'Hare, M., Venkateswaran, R., Liu, J., Michalak, Z., Ellis, M., Scheffer, I.E., Diehl, B., Sisodiya, S.M., Thom, M., 2018. The ventrolateral medulla and medullary raphe in sudden unexpected death in epilepsy. Brain 141, 1719–1733.

Power, J.D., Barnes, K.A., Snyder, A.Z., Schlaggar, B.L., Petersen, S.E., 2012. Spurious but systematic correlations in functional connectivity MRI networks arise from subject motion. Neuroimage 59, 2142–2154.

Puig, M.V., Gener, T., 2015. Serotonin modulation of prefronto-hippocampal rhythms in health and disease. ACS Chem. Neurosci. 6, 1017–1025.

Rubinov, M., Sporns, O., 2011. Weight-conserving characterization of complex functional brain networks. Neuroimage 56, 2068–2079.

Ryvlin, P., Nashef, L., Lhatoo, S.D., Bateman, L.M., Bird, J., Bleasel, A., Boon, P., Crespel, A., Dworetzky, B.A., Høgenhaven, H., Lerche, H., Maillard, L., Malter, M.P., Marchal, C., Murthy, J.M., Nitsche, M., Pataraia, E., Rabben, T., Rheims, S., Sadzot, B., Schulze-Bonhage, A., Seyal, M., So, E.L., Spitz, M., Szucs, A., Tan, M., Tao, J.X., Tomson, T., 2013. Incidence and mechanisms of cardiorespiratory arrests in epilepsy monitoring units (MORTEMUS): a retrospective study. Lancet Neurol. 12, 966–977.

Ryvlin, P., Rheims, S., Lhatoo, S.D., 2019. Risks and predictive biomarkers of sudden unexpected death in epilepsy patient. Curr. Opin. Neurol. https://doi.org/10.1997/WCO.0000000000000668.

Safaai, H., Neves, R., Eschenko, O., Logothetis, N.K., Panzeri, S., 2015. Modeling the effect of locus coeruleus firing on cortical state dynamics and single-trial sensory processing. Proc Natl.Acad Sci USA 112, 12834–12839.

Sveinsson, O., Andersson, T., Carlsson, S., Tomson, T., 2017. The incidence of SUDEP. A nationwide population-based cohort study. Neurology 89, 1–8.

Thurman, D.J., Hesdorffer, D.C., French, J.A., 2014. Sudden unexpected death in epilepsy: assessing the public health burden. Epilepsia 55, 1479–1485.

Venkatraman, A., Edlow, B.L., Immordino-Yang, M.H., 2017. The brainstem in emotion: a review. Front. Neuroanat. https://doi.org/10.3389/fnana.2017.00015.

Whelan, C.D., Altmann, A., Botia, J.A., Jahanshad, N., Hibar, D.P., Absil, J., Alhusaini, S., Alvim, M.K.M., Auvinen, P., Bartolini, E., Bergo, F.P.G., Bernardes, T., Blackmon, K., Braga, B., Caliguri, M.E., Calvo, A., Carr, S.J., Chen, J., Chen, S., Cherubini, A., David, P., Domin, M., Foley, S., Franca, W., Haaker, G., Isaev, D., Keller, S.S., Kotikalapudi,

R., Kowalczyk, M., Kuzniecky, R., Langner, S., Lenge, M., Leyden, K.M., Liu, M., Loi, R.Q., Rummel, C., Saavalainen, T., Semmelroch, M.K., Severino, M., Thomas, R.H., Tondelli, M., Tortora, D., Vaudang, A.E., Vivash, L., von Podewils, F., Wagner, J., Weber, B., Yao, Y., Yasuda, C.L., Zhang, G., Bargallo, N., Bender, B., Bernasconi, N., Bernasconi, A., Berhardt, B.C., Blümcke, I., Carlson, C., Cavalleri, G.L., Cendes, F., Concha, L., Delanty, N., Depondt, C., Devinsiky, O., Doherty, C.P., Focke, N.K., Gambardella, A., Guerrini, R., Hamandi, K., Jackson, G.D., Kälviäinen, R., Kochunov, P., Kwan, P., Labate, A., McDonald, C.R., Meletti, S., O'Brien, T.J., Ourselin, S., Richardson, M.P., Striano, P., Thesen, T., Wiest, R., Zhang, J., Vezzani, A., Ryten, M., Thompson, P.M., Sisodiya, S.M., 2018. Structural brain abnormalities in common epilepsies assessed in a worldwide enigma study. Brain 141, 391–408.

Whitfield-Gabrieli, S., Nieto-Castanon, A., 2012. Conn: a functional connectivity toolbox for correlated and anticorrelated brain networks. Brain Connect 2, 125–141.

Zhang, H., Zhao, H., Zeng, C., Van Dort, C., Faingold, C.L., Taylor, N.E., Solt, K., Feng, H.J., 2018. Optogenetic activation of 5-HT neurons in the dorsal raphe suppresses seizure-induced respiratory arrest and produces anticonvulsant effect in the DBA/1 mouse SUDEP model. Neurobiol. Dis. 110, 47–58.